Energy & Environmental Science

PAPER

View Article Online
View Journal | View Issue

Cite this: *Energy Environ. Sci.*, 2019, **12**, 1000

Highly stable single Pt atomic sites anchored on aniline-stacked graphene for hydrogen evolution reaction†

Shenghua Ye,‡[a] Feiyan Luo,‡[a] Qianling Zhang,‡[a] Pingyu Zhang,[a] Tingting Xu,[a] Qi Wang,[c] Dongsheng He,[e] Licheng Guo,[a] Yu Zhang,[a] Chuanxin He,[a] Xiaoping Ouyang,[d] Meng Gu,*[c] Jianhong Liu*[a] and Xueliang Sun*[b]

Received 1st October 2018,
Accepted 12th December 2018

DOI: 10.1039/c8ee02888e

rsc.li/ees

Developing efficient and cost-effective electrocatalysts for hydrogen evolution reaction (HER) is highly desired for the hydrogen economy. In this study, we developed a facile microwave reduction method to synthesize single Pt atoms anchored on aniline-stacked graphene (Pt SASs/AG) with outstanding HER performance. Pt SASs/AG presents excellent HER activity with η = 12 mV at 10 mA cm^{-2} and a mass current density of 22 400 Ag_{Pt}^{-1} at η = 50 mV, which is 46 times higher than that of commercial 20 wt% Pt/C. Moreover, the Pt SASs/AG catalyst is highly active and more stable than Pt/C. X-ray absorption fine spectroscopy and density functional theory calculations demonstrated that the coordination of atomically isolated Pt with the nitrogen of aniline optimized the electronic structure of Pt and the hydrogen adsorption energy, eventually promoting HER activity. This study provides a new avenue for the development of single-atom Pt electrocatalysts with high activity and stability.

Broader context

Exploring low-cost and efficient electrocatalysts for hydrogen evolution reaction (HER) from water splitting is important for hydrogen production. Hydrogen is a renewable and clean fuel that has great potential for solving the energy crisis. At present, the precious metal Pt is still the most active candidate catalyst with negligible overpotential for HER. However, the high cost and limited reserves of Pt hinder the commercialization of Pt-based catalysts. Thus, lowering the Pt loading of catalysts without sacrificing HER catalytic activity is an urgent goal. Single-atom catalysts (SACs) with isolated catalytic sites provide an alternative way to solve the above problems. However, the harsh preparation conditions (calcination or H_2 reduction) and excess precursors usually result in agglomeration, hindering the stability of SACs. Herein, for the first time, we present a mild and facile strategy that involves aniline anchoring and microwave reduction to exclusively disperse Pt atomic sites on graphene. Importantly, we demonstrate that the d-electron structure of Pt atoms can be modified by aniline molecules, which is crucial for improving HER activity. This study opens up a new avenue for developing SACs and provides a new understanding of the catalytic performances of SACs.

Introduction

Hydrogen is a promising candidate for green energy applications owing to its high energy density, low pollution and greenhouse gas-free emission.[1–3] Along with the popularization of electric energy, large-scale water splitting to generate high-purity hydrogen has attracted considerable attention, and many electrocatalysts for the hydrogen evolution reaction (HER) have been developed in recent years.[4]

Although Pt-based catalysts are the most active catalysts for HER,[5,6] the global reserves and high cost of Pt hinder their large-scale application.[7–9] In recent years, numerous catalysts made of non-noble transition metals have been explored for HER, such as transition metal phosphides,[10–12] sulfides,[13–16] nitrides,[17] selenides,[18–20] and carbides[21] due to their improved HER performances. Unfortunately, these transition metal catalysts usually have higher overpotential and lower catalytic performance compared to Pt-based catalysts. For these reasons, Pt remains irreplaceable at present. Until non-Pt-based catalysts are developed, it is important to find a method to drastically reduce Pt loading and improve catalytic activity.

[a] College of Chemistry and Environmental Engineering, Shenzhen University, Shenzhen, 518060, P. R. China. E-mail: liujh@szu.edu.cn
[b] Department of Mechanical and Materials Engineering, University of Western Ontario, London, Ontario N6A 5B9, Canada. E-mail: xsun9@uwo.ca
[c] Department of Materials Science and Engineering, Southern University of Science and Technology, Shenzhen, 518055, China. E-mail: gum@sustc.edu.cn
[d] School of Materials Science and Engineering, Xiangtan University, Xiangtan, 411105, P. R. China. E-mail: oyxp2003@yahoo.com.cn
[e] Materials Characterization and Preparation Center, South University of Science and Technology of China, Shenzhen, 518055, P. R. China

† Electronic supplementary information (ESI) available. See DOI: 10.1039/c8ee02888e

‡ These authors have contributed equally.

Recently, single-atom catalysts have attracted considerable attention because of their excellent catalytic performances.[22,23] For the first time, Zhang *et al.* demonstrated that single Pt atom dopants in FeO_x are well suited for CO oxidation and nitroarene hydrogenation.[24] Subsequently, other kinds of single atoms dispersed on g-C_3N_4,[25] ZnO,[26] Al_2O_3,[27] MoS_2,[28] CeO_2,[29] MoC,[30] and carbon substrates derived from polymers or metal–organic frameworks[31–38] have been developed as potential electrocatalysts. However, the preparation of single-atom catalysts requires harsh conditions and precise precursor concentrations. Calcination or H_2 reduction and excess precursors usually cause the single-atomic sites to form clusters or even nanoparticles during preparation.

In this study, single Pt atomic sites anchored on aniline-stacked graphene (denoted as Pt SASs/AG) were synthesized *via* a mild and facile process involving aniline anchoring and microwave reduction. The as-prepared catalyst with a Pt loading of 0.44 wt% presents an unexpectedly high catalytic activity with negligible onset potential and delivers an overpotential of 12 mV at 10 mA cm^{-2} in 0.5 M H_2SO_4 solution. Moreover, it displays excellent stability and durability without any obvious current deterioration or structural changes during long-term catalysis. Extended X-ray absorption fine spectroscopy (EXAFS) suggests that a Pt site coordinates with four aniline molecules. Density functional theory (DFT) calculations suggest that the electronic structure of Pt is altered by the aniline molecules, causing the single Pt atomic sites to have appropriate hydrogen adsorption energy. Furthermore, the Pt SASs/AG greatly improves the utilization of catalytic sites, and the excellent conductivity of graphene along with the hydrophilic catalyst interface contribute to its excellent HER performance.

Results and discussion

The preparation of Pt SASs/AG is depicted in Fig. 1. Graphene was functionalized by aniline molecules *via* π–π interactions. As a result, graphene became hydrophilic (the water contact angles before and after aniline stacking are shown in Fig. S3, ESI†) and thus could be uniformly re-dispersed in aqueous solution (Fig. S4, ESI†). Previous studies revealed that π–π interactions are strong and thus prevent stacked molecules from detaching into solution during electrocatalysis.[39,40] In particular, aromatic π–π interactions have two configurations: face-to-face and edge-to-face configurations. The absorption energies of these configurations were investigated by DFT. The results indicate that aniline stacked on graphene in the edge-to-face configuration has a significant lower energy than the face-to-face configuration (Fig. 1). Therefore, the edge-to-face configuration is thermodynamically preferred. Subsequently, H_2PtCl_6 solution (1 mL, 0.0193 mol L^{-1}) was added to the above solution and stirred for 2 h. During this process, the pH of the solution was 2.26, much lower than the pK_a (4.62) of the conjugate acid of aniline (the pK_b of aniline is 9.38). Thus, some of the $-NH_2$ groups of aniline were protonated to form $-NH_3^+$. Graphene was positively charged, and $PtCl_6^{2-}$ ions were electrostatically anchored on AG to maintain charge balance. Eventually, the anchored $PtCl_6^{2-}$ ions were reduced to single Pt atomic sites by microwave irradiation.

The transmission electron microscopy (TEM) images of Pt SASs/AG (Fig. 2a) demonstrate that the wrinkled structure of graphene is well maintained in Pt SASs/AG. The N and Pt elemental maps confirm that aniline and Pt are uniformly dispersed throughout the graphene in Pt SASs/AG (Fig. 2b). No nanoparticles or even clusters are observed on the surface of Pt SASs/AG (Fig. 2c and d). Aberration-corrected high-angle annular dark-field scanning TEM (AC HAADF-STEM) was used to characterize the dispersion of Pt in Pt SASs/AG. As illustrated in Fig. 2e and f, single Pt atomic sites (bright dots in Fig. 2e and f) were anchored on graphene without visible agglomeration, suggesting that atomically isolated Pt sites were obtained. The percentage of Pt in Pt SASs/AG measured by inductively coupled plasma-mass spectroscopy (ICP-MS) was 0.44 wt%.

The X-ray diffraction pattern of Pt SASs/AG (Fig. S6, ESI†) suggests that crystalline Pt is absent. X-ray photoelectron spectroscopy (XPS) indicated the presence of only C, N and O in AG (Fig. S7, ESI†). The C 1s spectrum suggests the presence of sp^2-hybridized carbon atoms, indicating planar graphene

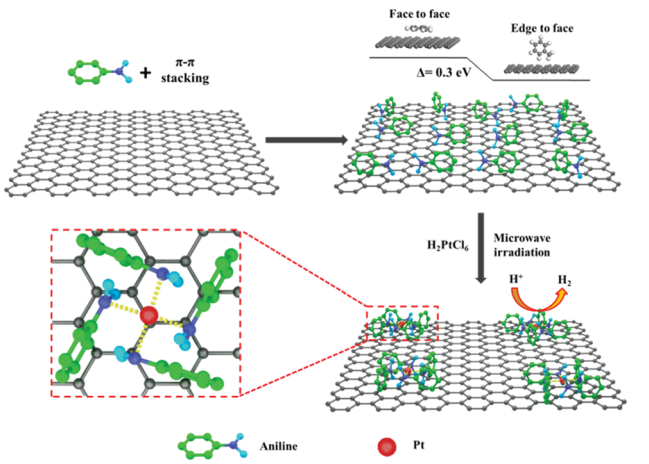

Fig. 1 Synthetic scheme of Pt SASs/AG.

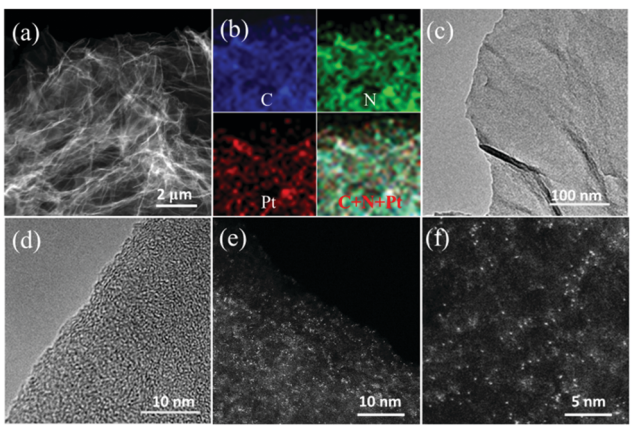

Fig. 2 (a) Low-magnification dark-field TEM image of Pt SASs/AG and (b) corresponding elemental maps of C, N and Pt. (c) High-magnification bright-field TEM image and (d) HR-TEM image of Pt SASs/AG. (e and f) AC HAADF-STEM images of Pt SASs/AG.

with a low defect concentration. The O 1s peak at ~532 eV is ascribed to adsorbed H_2O.[41,42] The trace amounts of N originated from the $-NH_2$ groups of stacked aniline. With the exception of the trace amounts of Pt, similar results were found for Pt SASs/AG (Fig. S8, ESI†). The content of N was calculated to be 2.75 at%. The Pt 4f spectrum of Pt SASs/AG in Fig. 3a suggests that the binding energy of Pt (71.55 eV) is close to that of Pt^0 (71.11 eV) with a slightly positive shift. The binding energy of Pt is far lower than that of Pt before microwave irradiation (72.8 eV; Fig. S9e, ESI†), suggesting that H_2PtCl_6 was reduced, and that the strong interaction between Pt and aniline formed $Pt^{\delta+}$. The Pt L_3-edge X-ray absorption near-edge structure (XANES) spectra of Pt SASs/AG, Pt/C, and Pt foil are shown in Fig. 3b. The white line (WL) has been reported to be directly related to the unoccupied density of states of the Pt 5d orbitals.[43,44] The intensive WL of Pt SASs/AG suggests increased vacancies in the d-orbitals of Pt and agrees with the XPS results. The EXAFS spectra of Pt SASs/AG, Pt/C, and Pt foil are shown in Fig. S10, ESI.† The Pt SASs/AG spectrum exhibits different oscillations than the Pt/C spectrum, suggesting different modes of coordination. The corresponding k^3-weight Fourier transforms (FTs) of the EXAFS spectra are depicted in Fig. 3c. The FT of Pt SASs/AG has only one peak corresponding to first-shell Pt–N coordination, and no Pt–Pt coordination peak is detected. Combined with the AC HAADF-STEM results, we can confidently conclude that atomically isolated Pt sites are dispersed on graphene. The obtained coordination number of Pt–N is about 4 (Table S1, ESI†), and the fitting curve (Fig. 3d) suggests that atomically isolated Pt is coordinated by four aniline molecules to form a Pt–N configuration, as illustrated in the inset of Fig. 3d.

Moreover, a series of Pt SASs/AG samples was prepared using different volumes (0–5 mL) of H_2PtCl_6 solution, and the loading amounts of Pt were measured by ICP-MS (Fig. 4a). The percentage of Pt increased from 0 to 0.44 wt% with increasing volume of H_2PtCl_6 solution and then remained constant at volumes above 1 mL. The AC-HAADF-STEM images (Fig. 4b–f) indicate that the Pt in all the above samples is present in single-atomic sites without visible agglomeration, indicating that anchoring to aniline results in the exclusive formation of single-atomic sites, even when excess metallic precursor was used. This finding differs from previous reports, in which clusters formed easily, and a precise amount of precursor was needed. This provides two main advantages. First, the maximum protonation of aniline results in the maximum loading of $PtCl_6^{2-}$, preventing excess Pt from being anchored. This guarantees that Pt clusters or nanoparticles cannot be formed, and 0.44 wt% is the saturated Pt loading of the Pt SASs. Second, microwave reduction is a mild synthetic method that does not require extreme conditions such as high temperature, which prevents the sintering of Pt SASs.

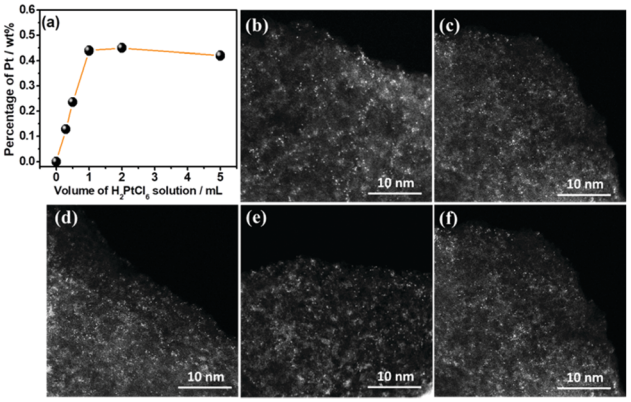

Fig. 4 (a) Mass percentages of Pt in Pt SASs/AG samples prepared by H_2PtCl_6 solution (0.3, 0.5, 1, 2, and 5 mL). AC-HAADF-STEM images of Pt SASs/AG samples prepared using (b) 0.3 mL, (c) 0.5 mL, (d) 1 mL, (e) 2 mL, and (f) 5 mL H_2PtCl_6 solution.

The electrocatalytic activity of Pt SASs/AG for HER in 0.5 M H_2SO_4 solution was evaluated by linear sweep voltammetry (LSV) at a scan rate of 2 mV s^{-1} with iR correction. The HER activities of Pt SASs/AG samples prepared using different concentrations of H_2PtCl_6 solution are depicted in Fig. S11, ESI.† The results agree with those shown in Fig. 4a, and the highest HER activity was observed at a Pt loading of 0.44 wt% (1 mL H_2PtCl_6 solution). Thus, the Pt SASs/AG with 0.44 wt% Pt was selected as a representative sample to further study the catalytic performance.

The LSV curves of Pt SASs/AG, AG and commercial 20 wt% Pt/C with *iR* correction are depicted in Fig. 5a (the LSV curves without iR correction are shown in Fig. S12, ESI†), indicating that Pt SASs/AG has a negligible onset potential. At the current density of 10 mA cm^{-2}, the Pt SASs/AG displays an overpotential of 12 mV, better than that of 20 wt% Pt/C (15 mV). To further compare the electrocatalytic activities of Pt SASs/AG and 20 wt% Pt/C, the current densities were normalized to the mass of Pt (Fig. 5b). The mass current density of Pt SASs/AG reaches 22 400 A g_{Pt}^{-1} at η = 50 mV, 46 times higher than that of 20 wt% Pt/C. Fig. 5c illustrates the mass activities of different Pt-based HER catalysts. Pt SASs/AG has a superior mass activity compared to other state-of-the-art Pt-based catalysts[45–50] and current Pt single-atom catalysts.[51–53] This suggests that the

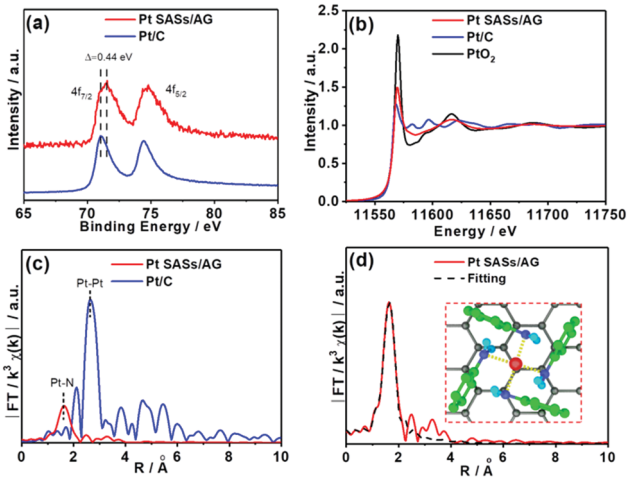

Fig. 3 (a) Pt 4f spectra of Pt SAS/AG and Pt/C. (b) XANES and (c) FT-EXAFS spectra of the Pt L_3-edge of Pt SASs/AG and Pt/C (without phase correction). (d) Corresponding EXAFS fitting curve of the Pt SASs/AG *R*-space. The inset shows the model of Pt SASs/AG.

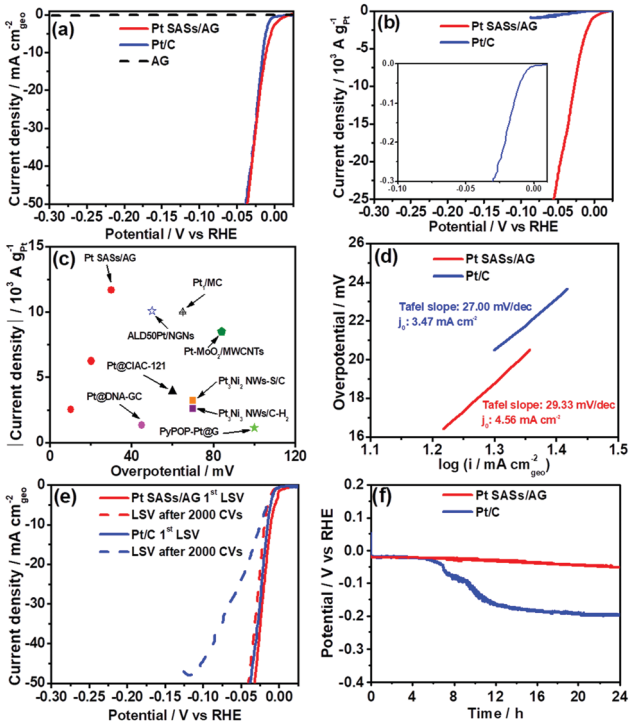

Fig. 5 LSV curves of Pt SASs/AG and Pt/C with current density normalized to the (a) geometry area and (b) mass of Pt in 0.5 M H_2SO_4 at 2 mV s^{-1} (inset shows the enlarged curves of Pt/C). (c) Mass activities of Pt SASs/AG, Pt/C, and other state-of-the-art Pt-based catalysts in 0.5 M H_2SO_4. (d) Tafel plots of Pt SASs/AG and Pt/C. (e) LSV curves of Pt SASs/AG before and after 2000 catalytic cycles. (f) Chronopotentiometric curves of Pt SASs/AG and Pt/C at 10 mA cm^{-2} in 0.5 M H_2SO_4 solution.

excellent catalytic activity with low Pt content is due to the unique single-atomic structure.

The Tafel slopes were calculated to identify the HER mechanism on the electrocatalysts (Fig. 5d). The Tafel slope of Pt SASs/AG is 29.33 mV dec^{-1}, close to that of Pt/C (27.00 mV dec^{-1}), suggesting a typical Tafel mechanism for HER.[54] By extrapolating the Tafel plots for η at 0 V, the exchange current density (j_0) of Pt SASs/AG was calculated to be 4.56 mA cm^{-2}, slightly higher than that of Pt/C (3.47 mA cm^{-2}). This suggests the high activity of Pt SASs/AG.

Stability is an important issue in the development single-atom electrocatalysts. The cyclic stabilities of Pt SASs/AG and Pt/C were evaluated by comparing the LSV curves before and after 2000 cycles (from +0.05 to −0.25 *vs.* RHE at 50 mV s^{-1}) in 0.5 M H_2SO_4 solution, as shown in Fig. 5e. Pt SASs/AG presents negligible decay in catalytic activity, whereas the 20 wt% commercial Pt/C deteriorates seriously after 2000 cyclic voltammetry sweeps. To further assess the long-term durability of Pt SASs/AG and Pt/C, chronopotentiometric measurements at a current density of 10 mA cm^{-2} were performed. The chronopotentiometric curves (Fig. 5f) of Pt SASs/AG and Pt/C suggest that Pt SASs/AG maintains its high catalytic activity and stability during long-term electrolysis, whereas Pt/C shows obvious attenuation. After durability testing, serious agglomeration occurs in Pt/C (Fig. S13, ESI†). Thus, the decreased activity of Pt/C can be attributed to the irreversible agglomeration of Pt nanoparticles driven by Ostwald ripening. In contrast, the TEM image of Pt SASs/AG after durability testing (Fig. S14a, ESI†) shows no clusters or nanoparticles on graphene; meanwhile, N and Pt remain uniformly dispersed on graphene (Fig. S14b–f, ESI†). The AC HAADF-STEM image shown in Fig. S14g, ESI† shows atomically dispersed Pt on most areas of the sample, even after long-term durability testing. Moreover, the electronic and coordination structures of Pt SASs/AG remain unchanged, as shown in Fig. S15 and Table S2, ESI.† The above sharp contrasts indicate that Pt SASs/AG has outstanding stability, which is ascribed to the strong interactions between Pt and aniline along with the strong π–π interactions of graphene.

The origin of the excellent HER activity of Pt SASs/AG was further investigated.

Visually, atomically dispersed sites maximize the utilization of Pt and thus greatly decrease the precious metal loading and significantly increase the mass activity. The aniline anchoring prevents Pt sites from aggregating during the catalytic process, thus improving the stability.

To provide a theoretical understanding of the effect of aniline, DFT calculations were carried out to study the structure–property correlation between Pt coordination and electrocatalytic activity. Fig. 6a–c show three typical structures (top view) of Pt(111), single Pt atom absorbed on graphene (Pt_{ab}/G), Pt SASs/AG; their partial densities of states (PDOSs) of the 5d orbitals are shown in Fig. 6d–f, respectively (the total DOSs are shown in Fig. S18, ESI†). Comparing to the electronic structure of Pt(111) which exhibits a typical energy band characteristic, the electronic structure of Pt in Pt_{ab}/G and Pt SASs/AG largely retains their isolated atomic orbital characteristics. The PDOS of Pt SASs/AG is greatly different from that of Pt_{ab}/G, indicating that the electronic structure of Pt is significantly affected by adjoining aniline molecules. The d-band center model is a good descriptor of adsorbate–metal interactions. The downshift in the d-band center decreases the adsorption energy of H and facilitates the desorption of H from the catalyst surface for HER catalysis.[55] As a result, the d-band center of Pt in Pt_{ab}/G is calculated to be −1.805 eV, which is higher than that of Pt in Pt(111) (−2.687 eV; Fig. 6d and e). This implies that single Pt atoms adsorbed on graphene are inactive for HER. However, when the single Pt atoms are anchored by aniline molecules, the d-band center downshifts to −2.465 eV, close to that of Pt(111) (Fig. 6f). This indicates that the synergetic effect of aniline and Pt is crucial for HER activity.

On the other hand, the DOS near the Fermi level is also crucial for the interaction of adsorbates (*e.g.*, H^+ for HER) with catalytic sites. High electron densities near the Fermi level can facilitate H^+ absorption.[56,57] The DOS near the Fermi level of Pt in Pt_{ab}/G is absent, again suggesting that Pt_{ab}/G is inactive for HER. Nevertheless, the DOS near the Fermi level of Pt in Pt SASs/AG is as large as that of Pt in Pt(111), indicating that the special coordination environment can effectively improve the d-electron density of Pt at the Fermi level thus optimize the catalytic activity.

Furthermore, the free energy of hydrogen adsorption (ΔG_H^*) is also a key factor in HER activity. HER can be summarized in a three-state diagram consisting of initial H^+, intermediate H atoms, and final H_2 as the product. The optimal ΔG_H^* of catalyst-H* is

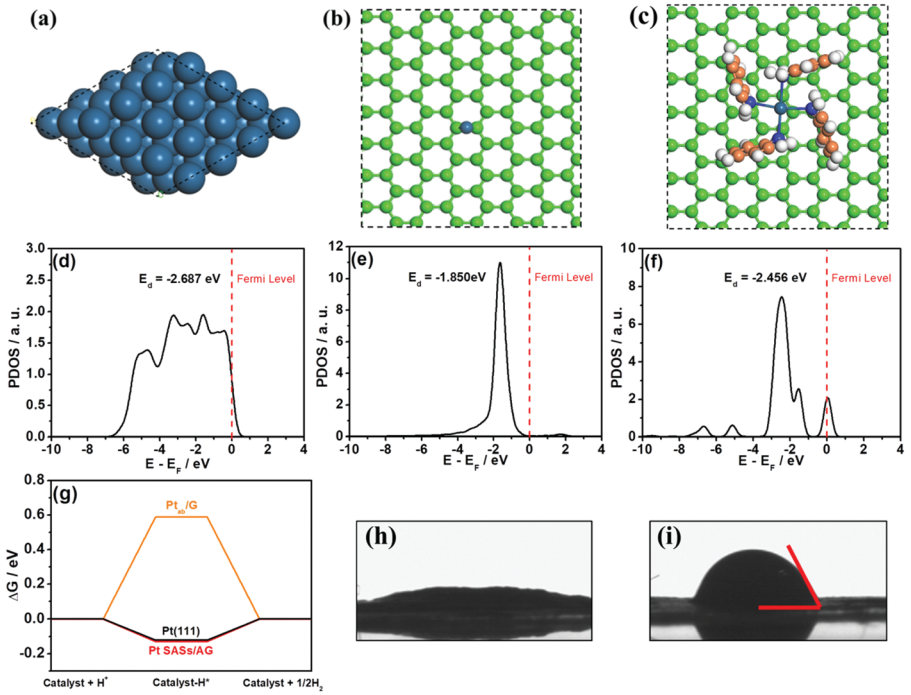

Fig. 6 DFT calculation models (top views) of (a) Pt(111), (b) Pt_{ab}/G and (c) Pt SASs/AG. PDOSs of the 5d orbitals of Pt in (d) Pt(111), (e) Pt_{ab}/G and (f) Pt SASs/AG. (g) Calculated free energy diagrams of HER for Pt(111), Pt_{ab}/G and Pt SASs/AG. Water contact angles of (h) Pt SASs/AG and (i) Pt/C.

close to 0 eV because a negative or positive ΔG_H^* on the catalyst will result in poor HER activity owing to difficulties in the desorption or generation of intermediate H atoms, respectively.[58,59] Simplified DFT models of Pt SASs/AG, Pt, and aniline are depicted in Fig. S19, ESI.† The ΔG_H^* diagrams of Pt SASs/AG, Pt_{ab}/G, and Pt(111) are shown in Fig. 6g. The calculated ΔG_H^* of Pt_{ab}/G is 0.587 eV, suggesting that single Pt atom alone on graphene is inactive for HER. In contrast, the ΔG_H^* of Pt SASs/AG is −0.127 eV, almost the same as that of Pt(111) (−0.121 eV). This confirms that coordination with aniline endows the single-atom Pt sites with HER activity, in agreement with the PDOS results.

Moreover, the electrical conductivities of Pt SASs/AG and Pt/C were determined using the four-probe method. The Pt SASs/AG resistivity is 1.22×10^{-2} Ω cm, which is remarkably lower than that of 20 wt% Pt/C (1.23 Ω cm). This is attributed to the higher conductivity of graphene compared to amorphous carbon, which favors electron transport and reduces the overpotential. In addition, the water contact angles of Pt SASs/AG and 20 wt% Pt/C (Fig. 6h and i) suggest that the Pt SASs/AG interface is more hydrophilic than that of 20 wt% Pt/C due to the stacking of aniline molecules on graphene. The hydrophilic interface ensures that the catalyst can be adequately wetted and penetrated by the electrolyte, which facilitates the diffusion and transport of active species.

Conclusions

In summary, we developed a facile method involving aniline anchoring and microwave reduction to synthesize single-atom Pt sites anchored on aniline-stacked graphene (Pt SASs/AG) for HER. Pt SASs/AG presents outstanding HER catalytic performances with higher specific current density and mass current density at lower overpotential and superior stability compared to 20 wt% Pt/C. The excellent HER activity of Pt SASs/AG is attributed to (1) the atomically dispersed Pt sites, which maximize the utilization of catalytic sites; (2) the modulation of the d-band center and DOS near the Fermi level of Pt atoms by aniline, which optimized the Gibbs free energy of H absorption; (3) the excellent electrical conductivity of graphene; and (4) the improved hydrophilicity of the catalyst interface owing to the stacking of aniline on graphene *via* π–π interactions. These findings provide a new opportunity for the preparation and application of high-efficiency and stable single-atom Pt sites for HER catalysis.

Experimental methods

Materials

Chemical reagents were all analytical grade and were used directly without purification. Chloroplatinic acid hexahydrate (H_2PtCl_6) and aniline were purchased from Aladdin. Ethylene glycol and anhydrous ethanol were purchased from Macklin. Single-layer graphene was produced by Shenzhen Eigen-equation Graphene Technology Co. Ltd (Shenzhen, China) *via* liquid sintering of liquid acrylonitrile homopolymer precursor.

Catalyst preparation

To prepare Pt SASs/AG, 10 mg graphene was mixed with 1 mL aniline and shook to form a black paste. Subsequently, 50 mL deionized water was used to uniformly disperse the paste. The dispersion was then filtered to obtain a black paste, re-dispersed

in deionized water, and filtered several times to remove the unstacked aniline and obtain aniline-stacked graphene. The aniline-stacked graphene was re-dispersed in 50 mL deionized water to form a uniform dispersion. Different volumes of 0.0193 mol L^{-1} H_2PtCl_6 were then added into the dispersion and vigorously stirred for 2 h. Next, the dispersion was filtered and re-dispersed in deionized water. This step was repeated more than ten times to thoroughly remove unanchored $PtCl_6^{2-}$ ions. The final product was dried overnight in a vacuum oven at 60 °C. The above product was re-dispersed in 10 mL ethylene glycol and subjected to 800 W microwave irradiation for 2 min. After cooling to room temperature, the sample was washed with deionized water and dried overnight in a vacuum oven at 60 °C to obtain Pt SASs/AG. To prepare AG, the same scheme applied for Pt SASs/AG was followed excluding the addition of H_2PtCl_6 and the microwave irradiation.

Catalyst characterization

The morphologies of the samples were characterized by TEM (JEM-2010HR and Tecnai F30 S-TWIN). The chemical states of samples were evaluated by XPS using an ESCAKAB 250 X-ray photoelectron spectrometer. All peaks were corrected by the C 1s line at 284.4 eV as a standard followed by curve fitting and background subtraction. Chemical composition was determined by ICP-AES using a TJA IRIS (HR) spectrometer. The catalysts were also characterized by Raman spectroscopy (Renishaw). XANES measurements of the Pt L-edge were conducted on the 06ID superconducting wiggler-sourced hard X-ray microanalysis beamline at the 1W1B station of the Beijing Synchrotron Radiation Facility. Each spectrum was collected in transmission mode for comparison and monochromatic energy calibration. Single Pt atoms were measured by AC HAADF-STEM (Titan Cubed Themis G20).

Electrochemical measurement

Electrochemical measurements were performed with a CHI 660E electrochemical analyzer (CH Instruments, Inc., Shanghai) using a standard three-electrode system. A sample-coated glass carbon electrode was the working electrode, a graphite rod was the counter electrode, and a saturated calomel electrode (SCE) was the reference electrode. The catalyst loading was 7.07 mg cm^{-2}. In all measurements, the SCE reference electrode was calibrated with respect to the reversible hydrogen electrode (RHE). In H_2-saturated 0.5 M H_2SO_4, E(RHE) = E(SCE) + 0.242 V. LSV measurements were conducted in electrolyte at a scan rate of 2 mV s^{-1}. Cyclic voltammetry was conducted at a scan rate of 50 mV s^{-1}.

Computational methods

First principles calculations in the framework of DFT, including structural and electronic performances, were conducted using the Cambridge Sequential Total Energy Package (*i.e.*, CASTEP).[60] The exchange–correlation functional under the generalized gradient approximation[61] with norm-conserving pseudopotentials and the Perdew–Burke–Ernzerhof functional was adopted to describe electron–electron interactions.[62] An energy cutoff of 750 eV was used, and a k-point sampling set of 5 × 5 × 1 was tested for convergence. A force tolerance of 0.01 eV $Å^{-1}$, energy tolerance of 5.0×10^{-7} eV per atom and maximum displacement of 5.0×10^{-4} Å were considered. Each atom in the storage model was allowed to relax to the minimum enthalpy without any constraints. The vacuum space along the z direction was set to 15 Å, which is sufficient to avoid interactions between two neighboring images. The Grimme method for DFT-D2 correction was considered for all calculations.[63] After building models of Pt on graphite with and without modification by C6, H atom was absorbed on top of the Pt atom, and all atoms of the systems were relaxed. The Pt(111) surface was also built with the three fixed bottom atomic layers and three relaxed top atomic layers.

The adsorption energy ΔE of the H atom on the substrate surface was defined as

$$\Delta E = E_{H}* - (E* + E_{H}),$$

where *H and * denote the adsorption of H atom on the substrate and the bare substrate, respectively, and E_H denotes half of the energy of H_2.

The free energy change ΔG of the reaction was calculated as the difference between the free energies of the initial and final states as follows:

$$\Delta G = \Delta E + \Delta ZPE - T\Delta S,$$

where E is energy calculated by DFT, ZPE is the zero point energy, and S denotes the entropy. The value of ($\Delta ZPE - T\Delta S$) was 0.24 eV,[63] and $\Delta G = \Delta E + 0.24$ eV.

Conflicts of interest

There are no conflicts to declare.

Acknowledgements

JL thanks the NSFC (No. 21571131) and Key Project of Natural Science Foundation of Guangdong Province (No. 2014A030311028). QZ thanks the Shenzhen Basic Research Layout Project (No. 20170447) and Major Programs for Science and Technology Development of Shenzhen (No. XCL201110060). The authors thank Dr D.-S. He for assistance with AC HAADF-STEM measurements.

References

1 J. Yang, F. Zhang, X. Wang, D. He, G. Wu, Q. Yang, X. Hong, Y. Wu and Y. Li, *Angew. Chem., Int. Ed.*, 2016, **55**, 12854–12858.
2 B. W. Hao, Y. X. Bao, Y. Le, X. Y. Yu and X. W. Lou, *Nat. Commun.*, 2015, **6**, 6512.
3 J. Staszakjirkovský, C. D. Malliakas, P. P. Lopes, N. Danilovic, S. S. Kota, K. C. Chang, B. Genorio, D. Strmcnik, V. R. Stamenkovic and M. G. Kanatzidis, *Nat. Mater.*, 2015, **15**, 197.
4 P. Munnik, P. E. de Jongh and K. P. de Jong, *Chem. Rev.*, 2015, **115**, 6687–6718.
5 J. K. Norskov and C. H. Christensen, *Science*, 2006, **312**, 1322–1323.
6 L. Zhang, L. T. Roling, X. Wang, M. Vara, M. Chi, J. Liu, S.-I. Choi, J. Park, J. A. Herron, Z. Xie, M. Marvrikakis and Y. N. Xia, *Science*, 2015, **349**, 412–416.

7 G. Li, X. Wang, J. Fu, J. Li, M. G. Park, Y. Zhang, G. Lui and Z. Chen, *Angew. Chem., Int. Ed.*, 2016, **55**, 4977–4982.
8 E. J. Popczun, C. G. Read, C. W. Roske, N. S. Lewis and R. E. Schaak, *Angew. Chem., Int. Ed.*, 2014, **126**, 5531–5534.
9 L. Liao, S. Wang, J. Xiao, X. Bian, Y. Zhang, M. D. Scanlon, X. Hu, Y. Tang, B. Liu and H. H. Girault, *Energy Environ. Sci.*, 2013, **7**, 387–392.
10 E. J. Popczun, J. R. McKone, C. G. Read, A. J. Biacchi, A. M. Wiltrout, N. S. Lewis and R. E. Schaak, *J. Am. Chem. Soc.*, 2013, **135**, 9267–9270.
11 Q. Liu, J. Tian, W. Cui, P. Jiang, N. Cheng, A. M. Asiri and X. Sun, *Angew. Chem., Int. Ed.*, 2014, **126**, 6710–6714.
12 M. Cabán-Acevedo, M. L. Stone, J. Schmidt, J. G. Thomas, Q. Ding, H.-C. Chang, M.-L. Tsai, J.-H. He and S. Jin, *Nat. Mater.*, 2015, **14**, 1245.
13 Y. Yin, J. Han, Y. Zhang, X. Zhang, P. Xu, Q. Yuan, L. Samad, X. Wang, Y. Wang and Z. Zhang, *J. Am. Chem. Soc.*, 2016, **138**, 7965–7972.
14 X. Yu, Y. Feng, Y. Jeon, B. Guan, X. W. Lou and U. Paik, *Adv. Mater.*, 2016, **28**, 9006–9011.
15 L. Yu, B. Y. Xia, X. Wang and X. W. Lou, *Adv. Mater.*, 2016, **28**, 92–97.
16 J. Duan, S. Chen, B. A. Chambers, G. G. Andersson and S. Z. Qiao, *Adv. Mater.*, 2015, **27**, 4234–4241.
17 J. Xie, S. Li, X. Zhang, J. Zhang, R. Wang, H. Zhang, B. Pan and Y. Xie, *Chem. Sci.*, 2014, **5**, 4615–4620.
18 H. Zhou, F. Yu, Y. Huang, J. Sun, Z. Zhu, R. J. Nielsen, R. He, J. Bao, W. A. Goddard III, S. Chen and Z. Ren, *Nat. Commun.*, 2016, **7**, 12765.
19 Y. Liu, X. Hua, C. Xiao, T. Zhou, P. Huang, Z. Guo, B. Pan and Y. Xie, *J. Am. Chem. Soc.*, 2016, **138**, 5087–5092.
20 L. Liang, H. Cheng, F. Lei, J. Han, S. Gao, C. Wang, Y. Sun, S. Qamar, S. Wei and Y. Xie, *Angew. Chem., Int. Ed.*, 2015, **54**, 12004–12008.
21 F.-X. Ma, H. B. Wu, B. Y. Xia, C.-Y. Xu and X. W. D. Lou, *Angew. Chem., Int. Ed.*, 2015, **54**, 15395–15399.
22 C. Zhu, S. Fu, Q. Shi, D. Du and Y. Lin, *Angew. Chem., Int. Ed.*, 2017, **56**, 13944–13960.
23 H. Zhang, G. Liu, L. Shi and J. Ye, *Adv. Energy Mater.*, 2018, **8**, 1701343.
24 B. Qiao, A. Wang, X. Yang, L. F. Allard, Z. Jiang, Y. Cui, J. Liu, J. Li and T. Zhang, *Nat. Chem.*, 2011, **3**, 634.
25 G. Gao, Y. Jiao, E. R. Waclawik and A. Du, *J. Am. Chem. Soc.*, 2016, **138**, 6292–6297.
26 X.-K. Gu, B. Qiao, C.-Q. Huang, W.-C. Ding, K. Sun, E. Zhan, T. Zhang, J. Liu and W.-X. Li, *ACS Catal.*, 2014, **4**, 3886–3890.
27 M. Moses-DeBusk, M. Yoon, L. F. Allard, D. R. Mullins, Z. Wu, X. Yang, G. Veith, G. M. Stocks and C. K. Narula, *J. Am. Chem. Soc.*, 2013, **135**, 12634–12645.
28 J. Deng, H. Li, J. Xiao, Y. Tu, D. Deng, H. Yang, H. Tian, J. Li, P. Ren and X. Bao, *Energy Environ. Sci.*, 2015, **8**, 1594–1601.
29 J. Jones, H. Xiong, A. T. DeLaRiva, E. J. Peterson, H. Pham, S. R. Challa, G. Qi, S. Oh, M. H. Wiebenga, X. I. P. Hernández, Y. Wang and A. K. Datye, *Science*, 2016, **353**, 150–154.
30 L. Lin, W. Zhou, R. Gao, S. Yao, X. Zhang, W. Xu, S. Zheng, Z. Jiang, Q. Yu and Y.-W. Li, *Nature*, 2017, **544**, 80.
31 Y. Han, Y.-G. Wang, W. Chen, R. Xu, L. Zheng, J. Zhang, J. Luo, R.-A. Shen, Y. Zhu, W.-C. Cheong, C. Chen, Q. Peng, D. Wang and Y. Li, *J. Am. Chem. Soc.*, 2017, **139**, 17269–17272.
32 J. Wang, Z. Huang, W. Liu, C. Chang, H. Tang, Z. Li, W. Chen, C. Jia, S. Wei and Y. Li, *J. Am. Chem. Soc.*, 2017, **139**, 17281–17284.
33 Y. Chen, S. Ji, Y. Wang, J. Dong, W. Chen, Z. Li, R. Shen, L. Zhen, Z. Zhuang, D. Wang and Y. Li, *Angew. Chem., Int. Ed.*, 2017, **56**, 6937–6941.
34 M. Zhang, Y.-G. Wang, W. Chen, J. Dong, L. Zheng, J. Luo, J. Wan, S. Tian, W.-C. Cheong, D. Wang and Y. Li, *J. Am. Chem. Soc.*, 2017, **139**, 10976–10979.
35 W. Chen, J. Pei, C.-T. He, J. Wan, H. Ren, Y. Zhu, Y. Wang, J. Dong, S. Tian, W.-C. Cheong, S. Lu, L. Zheng, W. Yan, Z. Zhuang, C. Chen, Q. Peng, D. Wang and Y. Li, *Angew. Chem., Int. Ed.*, 2017, **56**, 16086–16090.
36 C. J. Lei, Y. Wang, Y. Hou, P. Liu, J. Yang, T. Zhang, X. D. Zhuang, M. W. Chen, B. Yang, L. C. Lei, C. Yuan and X. L. Feng, *Energy Environ. Sci.*, DOI: 10.1039/C8EE01841C.
37 Z. G. Geng, Y. Liu, X. D. Kong, P. Li, K. Li, Z. Y. Liu, J. J. Du, M. Shu, R. Si and J. Zeng, *Adv. Mater.*, 2018, **30**, 1803498.
38 Y. T. Qu, Z. J. Li, W. X. Chen, Y. Lin, T. W. Yuan, Z. K. Yang, C. M. Zhao, J. Wang, C. Zhao, X. Wang, F. Y. Zhou, Z. B. Zhuang, Y. Wu and Y. D. Li, *Nat. Catal.*, 2018, **1**, 781–786.
39 Y. Jiang, Y. Lu, X. Lv, D. Han, Q. Zhang, L. Niu and W. Chen, *ACS Catal.*, 2013, **3**, 1263–1271.
40 Y. Zhang, X. Fan, J. Jian, D. Yu, Z. Zhang and L. Dai, *Energy Environ. Sci.*, 2017, **10**, 2312–2317.
41 J. Bao, X. Zhang, B. Fan, J. Zhang, M. Zhou, W. Yang, X. Hu, H. Wang, B. Pan and Y. Xie, *Angew. Chem., Int. Ed.*, 2015, **127**, 7507–7512.
42 Y. E. Roginskaya, O. Morozova, E. Lubnin, Y. E. Ulitina, G. Lopukhova and S. Trasatti, *Langmuir*, 1997, **13**, 4621–4627.
43 A. Mansour, J. Cook Jr and D. Sayers, *J. Phys. Chem.*, 1984, **88**, 2330–2334.
44 T. Sham, S. Naftel and I. Coulthard, *J. Appl. Phys.*, 1996, **79**, 7134–7138.
45 P. Wang, X. Zhang, J. Zhang, S. Wan, S. Guo, G. Lu, J. Yao and X. Huang, *Nat. Commun.*, 2017, **8**, 14580.
46 S. Wang, X. Gao, X. Hang, X. Zhu, H. Han, W. Liao and W. Chen, *J. Am. Chem. Soc.*, 2016, **138**, 16236–16239.
47 X. Xie, Y.-F. Jiang, C.-Z. Yuan, N. Jiang, S.-J. Zhao, L. Jia and A.-W. Xu, *J. Phys. Chem. C*, 2017, **121**, 24979–24986.
48 S. Anantharaj, P. E. Karthik, B. Subramanian and S. Kundu, *ACS Catal.*, 2016, **6**, 4660–4672.
49 A. B. Soliman, M. H. Hassan, T. N. Huan, A. A. Abugable, W. A. Elmehalmey, S. G. Karakalos, M. Tsotsalas, M. Heinle, M. Elbahri, M. Fontecave and M. Alkordi, *ACS Catal.*, 2017, **7**, 7847–7854.
50 P. Wang, K. Jiang, G. Wang, J. Yao and X. Huang, *Angew. Chem., Int. Ed.*, 2016, **128**, 13051–13055.
51 N. Cheng, S. Stambula, D. Wang, M. Banis, T. Liu, A. Riese, B. Xiao, R. Li, T. Sham, M. Liu, G. Botton and X. Sun, *Nat. Commun.*, 2016, **7**, 13638.
52 H. Wei, K. Huang, D. Wang, R. Zhang, B. Ge, J. Ma, B. Wen, S. Zhang, Q. Li, M. Lei, C. Zhang, J. Irawan, L. Liu and H. Wu, *Nat. Commun.*, 2017, **8**, 1490.

53 X. Yin, H. Wang, S. Tang, X. Lu, M. Shu, R. Si and T. Lu., *Angew. Chem., Int. Ed.*, 2018, **57**, 9382–9386.
54 Y. Shi and B. Zhang, *Chem. Soc. Rev.*, 2016, **45**, 1529–1541.
55 Z. Chen, Y. Song, J. Cai, X. Zheng, D. Han, Y. Wu, Y. Zang, S. Niu, Y. Liu, J. Zhu, X. Liu and G. Wang, *Angew. Chem., Int. Ed.*, 2018, **57**, 5076–5080.
56 L. Zhang, Y. Jia, G. Gao, X. Yan, N. Chen, J. Chen, M. Soo, B. Wood, D. Yang, A. Du and X. Yao, *Chem*, 2018, **4**, 285–297.
57 W. Chen, J. Pei, C. He, J. Wan, H. Ren, Y. Zhu, Y. Wang, J. Dong, S. Tian, W. Cheong, S. Lu, L. Zheng, X. Zheng, W. Yan, Z. Zhuang, C. Chen, Q. Peng, D. Wang and Y. Li, *Angew. Chem., Int. Ed.*, 2017, **56**, 16086–16090.
58 Y. Jiao, Y. Zheng, K. Davey and S. Qiao, *Nat. Energy*, 2016, **1**, 16130.
59 Y. Jiao, Y. Zheng, M. Jaroniec and S. Qiao, *Chem. Soc. Rev.*, 2015, **44**, 2060–2068.
60 M. D. Segall, P. J. D. L. M. J. Probert, C. J. Pickard, P. J. Hasnip, S. J. Clark and M. C. Payne, *J. Phys.: Condens. Matter*, 2002, **14**, 2717–2744.
61 J. P. Perdew, K. Burke and M. Ernzerhof, *Phys. Rev. Lett.*, 1996, **77**, 3865–3868.
62 D. R. Hamann, M. Schlüter and C. Chiang, *Phys. Rev. Lett.*, 1979, **43**, 1494–1497.
63 D. Voiry, H. Yamaguchi, J. Li, R. Silva, D. C. B. Alves, T. Fujita, M. W. Chen, T. Asefa, V. Shenoy, G. Eda and M. Chhowalla, *Nat. Mater.*, 2013, **12**, 850–855.